

Multimode Fatigue Criteria for Filled Non-crystalizing Rubber under Positive R Ratios

Robert Keqi Luo 

Trelleborg Antivibration Solutions, Leicester LE4 2BN, UK

Received February 23 2023; Revised April 07 2023; Accepted for publication May 07 2023.

Corresponding author: R.K. Luo (Robert.luo@trelleborg.com; Luo0801@gmail.com)

© 2023 Published by Shahid Chamran University of Ahvaz

Abstract. Antivibration isolators are made from both crystalizing rubbers and non-crystalizing rubbers. Their fatigue resistance is different. Although the recently developed effective tensile stress criterion has been validated in crystalizing rubber under different R ratios (the ratio between the minimum stress value and the maximum stress value), its application to non-crystalizing rubbers has never been verified. In this study, this criterion was tested against a non-crystalizing rubber using two types of samples under $R \geq 0$ conditions for 168 fatigue cases with different loading modes. Considering that a shape change may also cause fatigue damage, a new shear stress criterion was derived and subsequently tested. The unified S-N curves ($2 \times 10^2 - 3 \times 10^6$ cycles) obtained have achieved narrow bands with a scatter factor of 1.35 with a correlation coefficient $R^2 \geq 0.90$ using these two criteria. This potential novel approach could be more effective than the current methods, which use fitting functions with adjustable parameters determined from an additional experiment. This offers greater choices and flexibility to engineers in their selection of the most appropriate suited criteria for their design in anti-vibration applications.

Keywords: Rubber fatigue; Effective shear stress; Effective tensile stress; Damage criteria; R ratio.

1. Introduction

Rubber isolators are widely used in dynamic environments such as trains, cars, and industrial equipment. The fatigue-life requirement must be met before the products can be accepted for service. In a design stage, a suitable fatigue criterion is required to evaluate the performance of a product. Many criteria have been developed for the evaluation of rubber fatigue, such as strain energy density [1-3], CED (cracking energy density) criterion [4-6], strain-based criteria [8-12] and stress-based criteria [13-16]. The above damage criteria were also used for engineering applications [17-20].

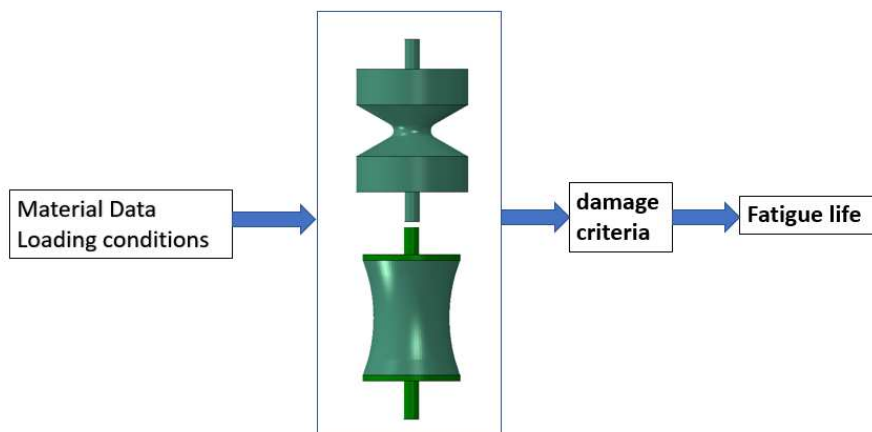


Fig. 1. The schematic configuration of the considered fatigue life approach.

However, when different R ratios (the ratio between the minimum stress/strain/load value and the maximum stress/strain/load value) are involved, additional tests and work are required for the modifications to the above criteria.

Mars and Fatemi [21], Wang et al. [22] and Ayoub et al. [23, 24] proposed damage criteria with fitting parameters to deal with different R ratios and made good progress. The limitation of their criteria is that the unknown parameters of their criteria need to be determined in relevant experiments for the specified material. Attempting to eliminate the limitation, Luo suggested an effective tensile stress criterion σ_t [25] to include the effect of the R ratios and successfully applied a type of strain crystallizing rubber, that is, a filled natural rubber.

Antivibration isolators can be made from either crystallizing rubbers or non-crystallizing rubbers. Their fatigue resistance is different. Although the tensile stress criterion σ_t , developed recently, has been validated in crystallizing rubber under different R ratios, its application to non-crystallizing rubbers has never been verified. In this study, this criterion was tested on a non-crystallizing rubber, i.e., filled SBR (Styrene-Butadiene Rubber). Considering that a shape change may also cause fatigue damage, a new shear stress criterion τ_t was derived and tested. If the approach is successful, the proposed criteria can be extended to a much wider range of industrial applications for different rubber materials. The rest of this article is organised in the following way: the presentation of the damage criteria is introduced, followed by their application to two different types of specimens. The predicted results are compared with the published experimental observations before a summary of the findings. The schematic configuration of the considered fatigue life approach is shown in Fig. 1.

2. Damage Criteria and Validation

2.1 Damage criteria

A damage criterion, effective tensile stress, was first proposed and applied to a filled natural rubber (crystallising rubber) in the literature [25]. For the reader's convenience, it is briefly described here.

The effective tensile stress σ_t is defined as a function of its three principal components σ_{ti} with equal weight:

$$\sigma_t = \sqrt{\sigma_{t1}^2 + \sigma_{t2}^2 + \sigma_{t3}^2} \quad \sigma_{ti} > 0, \quad \sigma_{t1} \geq \sigma_{t2} \geq \sigma_{t3} \tag{1}$$

The physical meaning of this stress definition is that the maximum fatigue damage needs to be calculated from all three principal tensile stresses rather than the maximum tensile stress alone. To calculate σ_{ti} , we assume that a point of a rubber component is subjected to a cyclic loading between a base stress σ_I and a current stress σ_{II} with a stress range $\Delta\sigma = \sigma_{II} - \sigma_I$, shown in Fig. 2. The direction of σ_{ti} is defined as the same direction of $\Delta\sigma_i$, shown in Fig. 3. The components σ_{ti} ($i = 1,2,3$) can be calculated based on the following criteria:

$$\sigma_{ti} = 0, \text{ if } \sigma_{IIi} \leq 0 \text{ or } \Delta\sigma_i \leq 0 \tag{2}$$

$$\sigma_{ti} = \Delta\sigma_i, \text{ if } \sigma_{IIi} \geq \Delta\sigma_i. \tag{3}$$

$$\sigma_{ti} = \sigma_{IIi}, \text{ if } \sigma_{IIi} < \Delta\sigma_i. \tag{4}$$

If the current stress $\sigma_{IIi} = 1$ MPa and the stress range $\Delta\sigma_i = 0.5$ MPa, then based on the equation (3), $\sigma_{ti} = 0.5$ MPa. If the current stress $\sigma_{IIi} = 1$ MPa and the stress range $\Delta\sigma_i = 2$ MPa, $\sigma_{ti} = 1$ MPa is obtained from the equation (4).

The direction of σ_t determines a failure plane of a fatigue crack. Let projections of σ_{ti} to three axes of a coordinate system be:

$$\sigma_{t1} = [\sigma_{t1i}, \sigma_{t1j}, \sigma_{t1k}], \sigma_{t2} = [\sigma_{t2i}, \sigma_{t2j}, \sigma_{t2k}], \sigma_{t3} = [\sigma_{t3i}, \sigma_{t3j}, \sigma_{t3k}] \tag{5}$$

Then the direction is as follows:

$$d = [d_i, d_j, d_k] \tag{6}$$

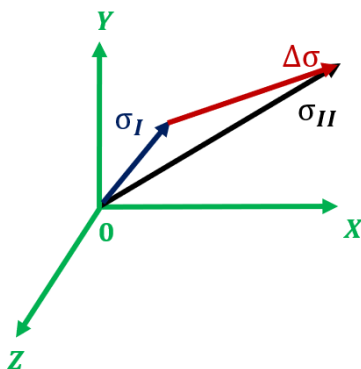


Fig. 2. Stress tensors during fatigue loading.

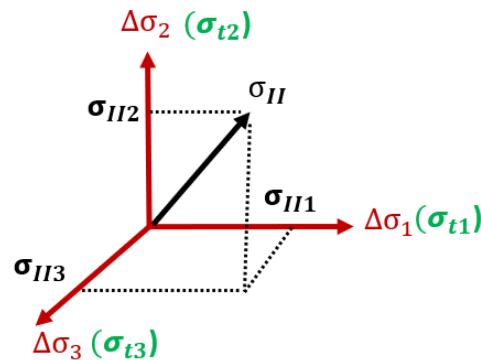


Fig. 3. Relationship between stress range, current stress, and effective tensile stress.



and if $\sigma_{t1}, \sigma_{t2}, \sigma_{t3} > 0$:

$$\begin{aligned}
 d_i &= (\sigma_{t1i} + \sigma_{t2i} + \sigma_{t3i})/\sigma_t \\
 d_j &= (\sigma_{t1j} + \sigma_{t2j} + \sigma_{t3j})/\sigma_t \\
 d_k &= (\sigma_{t1k} + \sigma_{t2k} + \sigma_{t3k})/\sigma_t
 \end{aligned}
 \tag{7}$$

The above relationship of the variables is shown in Fig. 4.

In addition to σ_t , we introduce a new damage criterion based on shape deformation caused by shear stresses. It is hypothesized that rubber fatigue damage can be initiated at a place where a shear parameter, the effective shear stress τ_t , reaches its maximum value. τ_t is defined as:

$$\tau_t = \sqrt{\tau_{t1}^2 + \tau_{t2}^2 + \tau_{t3}^2} \quad \tau_{t1} \geq \tau_{t2} \geq \tau_{t3}
 \tag{8}$$

where

$$\begin{aligned}
 \tau_{t1} &= 0.5(\sigma_{t1} - \sigma_{t3}) \\
 \tau_{t2} &= 0.5(\sigma_{t1} - \sigma_{t2}) \\
 \tau_{t3} &= 0.5(\sigma_{t2} - \sigma_{t3}) \quad (\tau_{t2} > \tau_{t3})
 \end{aligned}
 \tag{9}$$

The function (8) defines a spherical envelope in a rectangular coordinate system, shown in Fig. 5. Any point located on the surface represents the same fatigue damage. If τ_{t1} is considered only, expression (8) becomes the maximum shear stress criterion.

In industry, the hyperelastic approach is widely used to simulate the response of rubber isolators [26-28]. The main equations for a hyperelastic model based on the strain energy density are listed below.

The proposed criteria can be integrated with:

$$W = W_I(\bar{I}) + W_J(J)
 \tag{10}$$

where W is the strain energy density. W_I is related to the deviatoric mechanical behaviour of the material and W_J describes the volumetric behaviour of the material. \bar{I} is a set of the invariants of the left Cauchy-Green deformation tensor \mathbf{b} that can be expressed using the deformation gradient tensor \mathbf{F} :

$$\mathbf{F} = \begin{Bmatrix} 1 + \frac{\partial u_1}{\partial X_1} & \frac{\partial u_1}{\partial X_2} & \frac{\partial u_1}{\partial X_3} \\ \frac{\partial u_2}{\partial X_1} & 1 + \frac{\partial u_2}{\partial X_2} & \frac{\partial u_2}{\partial X_3} \\ \frac{\partial u_3}{\partial X_1} & \frac{\partial u_3}{\partial X_2} & 1 + \frac{\partial u_3}{\partial X_3} \end{Bmatrix}
 \tag{11}$$

$$\mathbf{b} = \mathbf{F} \bullet \mathbf{F}^T \quad (b_{ij} = F_{ik} F_{jk})
 \tag{12}$$

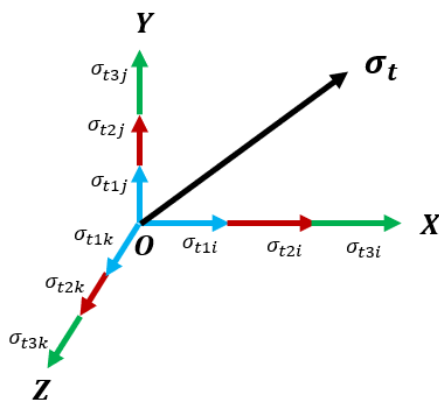


Fig. 4. The illustration for the direction of σ_t .

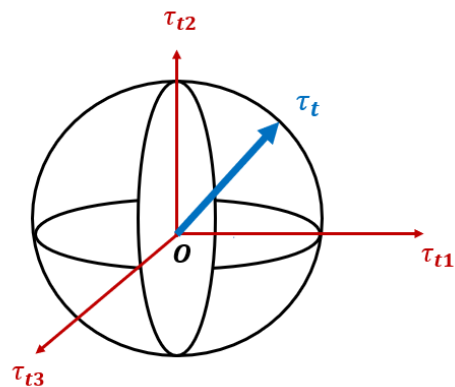


Fig. 5. Geometric meaning for τ_t .



The first part of \bar{I} :

$$\bar{I}_1 = \frac{I_1}{J^{2/3}} \tag{13}$$

$$I_1 = \text{trace}(\mathbf{b}) \tag{14}$$

where J is the Jacobian of the deformation gradient:

$$J = \sqrt{\det(\mathbf{b})} = \det(\mathbf{F}) \tag{15}$$

The second part of \bar{I} :

$$\bar{I}_2 = \frac{I_2}{J^{4/3}} \tag{16}$$

$$I_2 = \frac{1}{2}(I_1^2 - \mathbf{b} \bullet \mathbf{b}) \tag{17}$$

The stress-strain law can be obtained by differentiating the strain energy density W using standard methods, and the results are given below:

$$\sigma_{ij} = \frac{2}{J} \left[\frac{1}{J^{2/3}} \left(\frac{\partial W}{\partial I_1} + \bar{I}_1 \frac{\partial W}{\partial I_2} \right) b_{ij} - \left(\bar{I}_1 \frac{\partial W}{\partial I_1} + 2 \bar{I}_2 \frac{\partial W}{\partial I_2} \right) \frac{\delta_{ij}}{3} - \frac{1}{J^{4/3}} \frac{\partial W}{\partial I_2} b_{ik} b_{kj} \right] + \frac{\partial W}{\partial J} \delta_{ij} \tag{18}$$

where σ_{ij} are the components of the symmetric Cauchy stress tensor (true stresses) and δ_{ij} is the Kronecker delta.

2.2 Validation of Damage Criteria

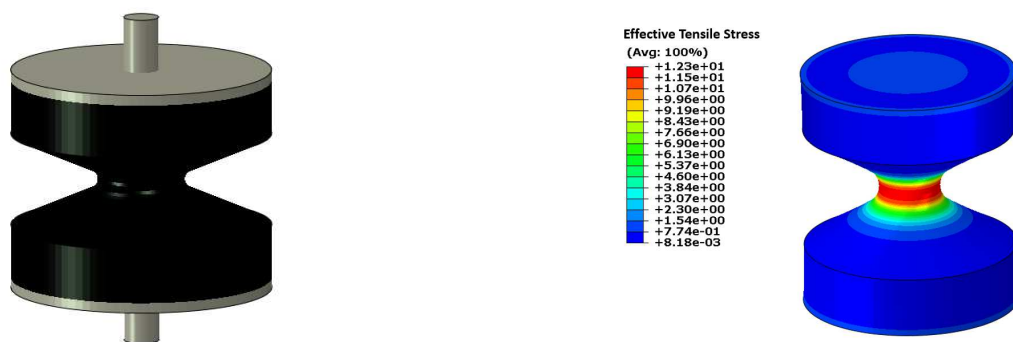
The experimental data published by Ayoub et al. [23, 24] are used to validate the proposed criteria. The data contain 168 fatigue cases with $R = 0$ and $R > 0$ for AE2 (the radius of the middle section is 2 mm) and $R = 0$ for AE42 (the radius of the middle section is 42 mm) specimens. Both types of specimens were made of the same SBR. The SBR material formulation can be found in reference [23]. The following sections describe the effect of loading modes, sample geometries, and correlations of fatigue damage results.

2.2.1 σ_t application for AE2 samples

The AE2 specimen was 30mm high and its middle section had a radius of 2 mm, as shown in Fig. 6 (a). A second order Ogden form was used to simulate the rubber response under the loadings with constants: $\mu_1 = 5.25$ MPa, $\mu_2 = 0.0152$ MPa, $\alpha_1 = 0.214$ and $\alpha_2 = 4.06$ [23]. ABAQUS software [27] was used to model the sample. Approximately 1100 elements were used to form an axisymmetric model after a mesh sensitivity analysis was performed. The type of element was CGAX4H. We first apply the calculation procedure of σ_t to AE2 samples.

To observe the response from different loading modes, a total of 33 fatigue cases ($R = 0$) were performed in tension, torsion, and tension + torsion tests [23]. For the tension loads, there were 8 cases; for the torsion loads, there were 13 cases; and for the combined tension-torsion cases, there were 12 cases. Figure 6 (b) shows a typical profile of σ_t under a combination between a tension load and a torsion load: tension 0 - 3.38 mm and torsion 0 - 60°. The critical location is in the middle section, which is consistent with the experimental observations. This location is the same as those of the 33 fatigue cases that contained 8 tension cases, 13 torsion cases, and 12 tension and torsion cases. A prediction of the effective tensile stress against cycle numbers is plotted in Fig. 7 (a). It is shown that the criterion unified the response of all different loading modes. The correlation coefficient was $R^2 = 0.96$ and the band scatter factor was 1.2.

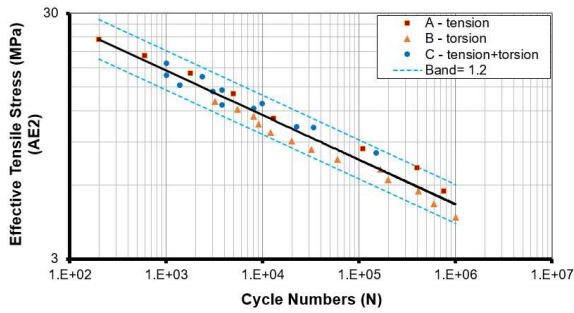
To observe the effect of R ratios, 43 fatigue loads were applied to AE2 in torsion experiments [23]. The R ratio (the ratio between the minimum stress value and the maximum stress value) was in a range of 0.04 to 0.64. The fatigue loads were divided into 6 groups, namely from D1 to D6. For the group D1, the angle difference was fixed to 50°. For the group D2, the angle difference was fixed to 70°. For the group D3, the angle difference was fixed to 100°. For the group D4, the maximum angle was fixed to 100°. For the group D5, the maximum angle was fixed to 80°. For the group D6, the maximum angle was fixed to 70°. Figure 7 (b) shows σ_t response of the fatigue loading conditions. It achieved a band factor of 1.2 with $R^2 = 0.97$.



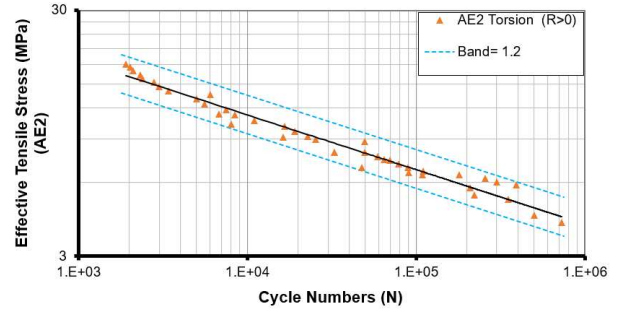
(a) AE2 specimen: the black colour is for rubber and the silver colour is for metal. (b) Profile of σ_t for the rubber part of the AE2 sample under tension 0 - 3.38 mm and torsion 0 - 60° with the failed number of 8000.

Fig. 6. The AE2 sample and a profile of σ_t .

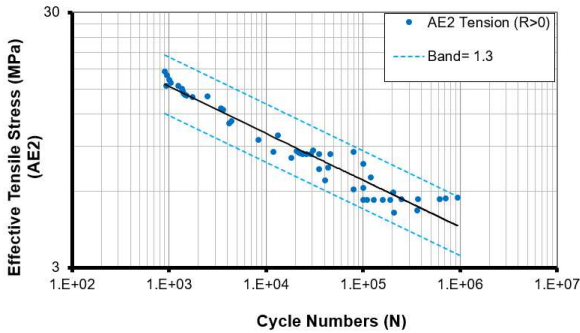




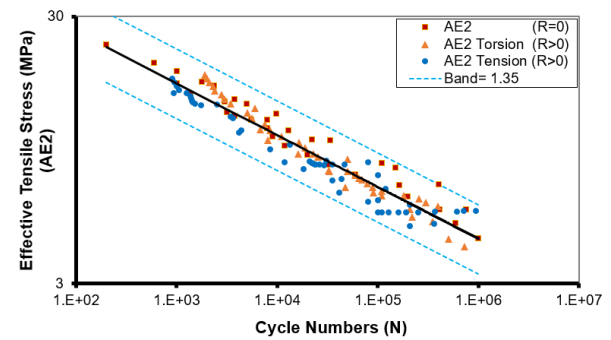
(a) σ_t response of the AE2 samples under 33 fatigue cases: tension, torsion, and tension + torsion, $R^2 = 0.96$. Black line – regression line.



(b) σ_t response of the AE2 samples under 43 fatigue cases ($R > 0$) in torsion, $R^2 = 0.97$. Black line – regression line.

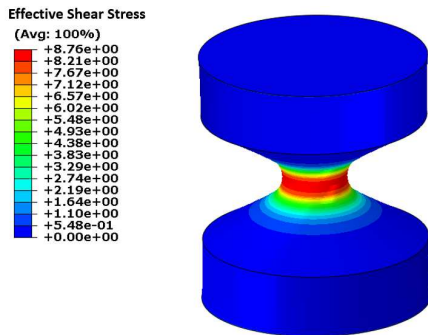


(c) σ_t response of the AE2 samples under 52 fatigue cases ($R > 0$) in tension, $R^2 = 0.96$. Black line – the regression line.

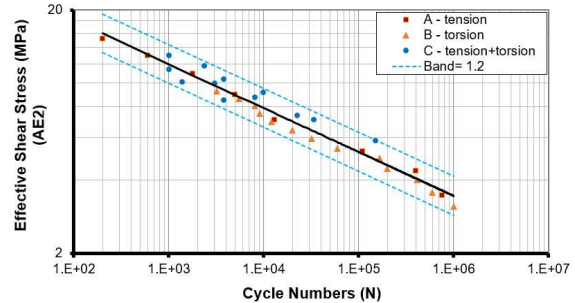


(d) σ_t response of the AE2 samples under 128 fatigue cases (different R-ratios), $R^2 = 0.94$. Black line – the regression line.

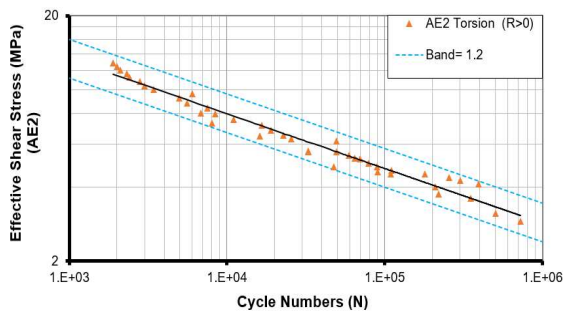
Fig. 7. σ_t response of the AE2 samples.



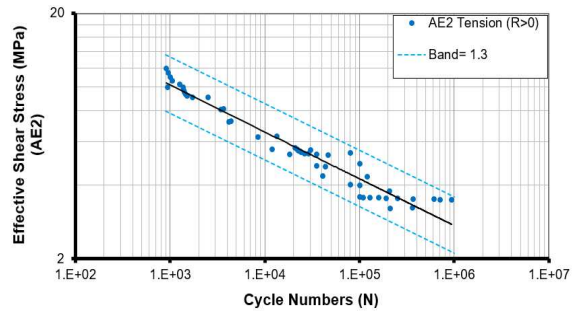
(a) Profile of τ_t in AE2 sample: tension 0 – 3.38 mm and torsion 0 - 60° with failed number of 8000.



(b) τ_t response of AE2 samples under 33 fatigue cases in tension, torsion, and tension + torsion, $R^2 = 0.96$. Black line – the regression line.



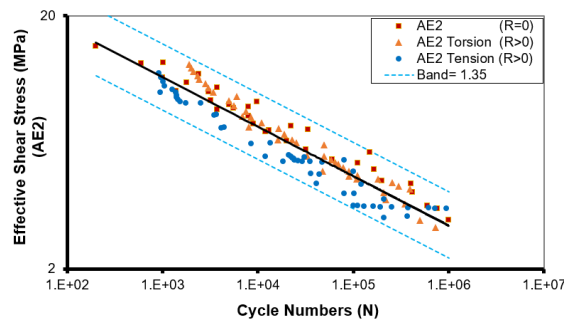
(c) τ_t response of AE2 samples under 43 fatigue cases ($R > 0$) in torsion: $R^2 = 0.97$. Black line – the regression line.



(d) τ_t response of AE2 samples under 52 fatigue cases ($R > 0$) in tension: $R^2 = 0.96$. Black line – the regression line.

Fig. 8. τ_t response of the AE2 samples.





(e) τ_t response of AE2 samples in 128 fatigue cases under different R ratios: $R^2 = 0.91$. Black line – the regression line.

Fig. 8. Continued.

The same procedure was applied to tension experiments of 52 cases in a range of $0.08 \leq R \leq 0.61$. There were 7 groups together. The group E1 to E3 had fixed difference 2.25 mm, 3.38 mm, and 5.63 mm, respectively. The group E4 to E7 had the maximum values in a range of 6.75 mm, 5.63 mm, 4.5 mm, and 3.8 mm. A band factor of 1.35 with $R^2 = 0.96$ was obtained, as shown in Fig. 7 (c). Since σ_t has unified the response of different loading modes with and without preloads, it is possible to combine each case together for all fatigue experiments. Figure 7 (d) summarised the results of all fatigue cases. A correlation coefficient $R^2 = 0.94$ with a band factor of 1.35 was achieved in 128 cases of fatigue under different R ratios. Therefore, the damage criterion σ_t seems to be suitable for AE2 samples made from SBR. It works well in different loading modes and R ratios.

2.2.2 τ_t application for AE2 samples

To compare the results of 2.2.1, we follow the same calculation procedure of σ_t to obtain responses of τ_t under the same conditions. Figure 8 (a) shows the profile of τ_t under the same load condition as in Fig. 6 (b). The maximum value of τ_t was in the same location of σ_t in Fig. 6 (b).

Figure 8 (b) plots 33 cases in different loading modes with $R^2 = 0.96$ and the scatter band 1.2, which is the same as in Fig. 7 (a). Similarly, the τ_t response of 43 fatigue cases under torsion and 52 cases under tension have achieved the same results as those from the σ_t response, as shown in Figs. 8 (c) and (d). Therefore, all 128 cases can be combined to obtain a unified τ_t response, shown in Fig. 8(e), which is the same as that obtained for σ_t . These two criteria have unified different loading modes and R ratios and achieved almost the same accuracy in AE2 specimens.

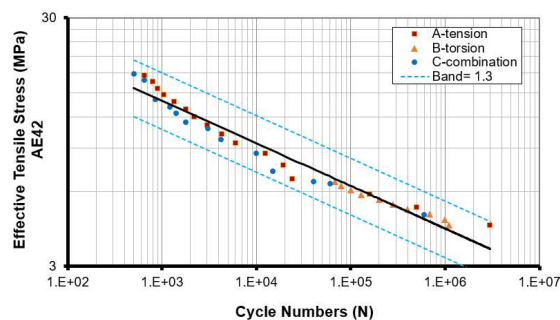
2.2.3 σ_t application for AE42 samples

In reference [24], AE42 samples, made from the same material as those in AE2 samples, were used to perform 40 fatigue tests in three loading modes ($R = 0$): tension, torsion, and tension + torsion. For the tension loads, there were 17 cases; for the torsion loads, there were 10 cases; and for the combined tension-torsion cases, there were 13 cases. The sample had 30 mm in height and 20 mm in mid-diameter, as shown in Fig. 9(a). Approximately 1000 elements were used for an axisymmetric model after a mesh sensitivity analysis. A profile of σ_t in a load case is shown in Fig. 9(b) and the maximum value is located in the mid-plane, which is observed in the test. Following the same calculation procedure for all load cases, the σ_t response is plotted in Fig. 9(c). A scatter band of 1.3 was achieved with $R^2 = 0.95$. Hence, the criterion of σ_t seems to be suitable for AE42 samples.



(a) The AE42 specimen: the black colour is for rubber and the silver colour is for metal.

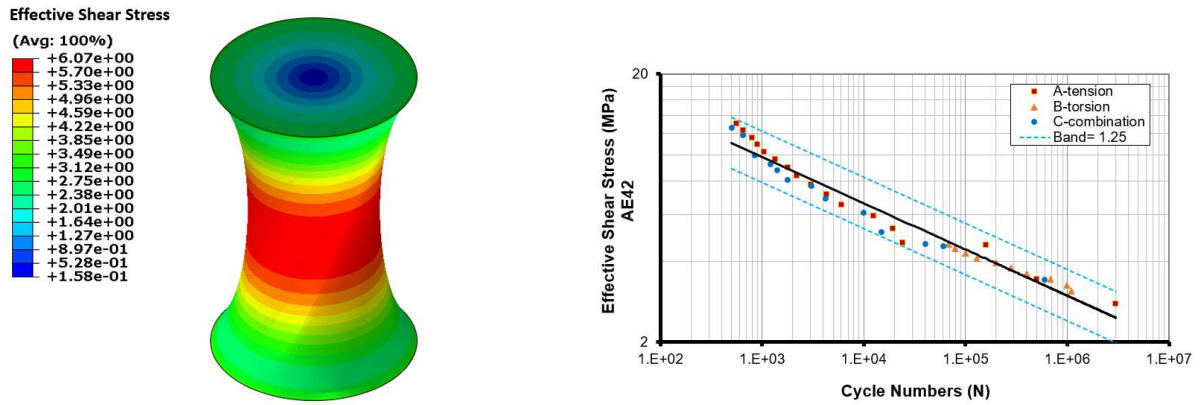
(b) Profile of σ_t for the rubber part of the AE42 sample under tension 0 - 9.8 mm and torsion 0 - 100° with failed number of 10000.



(c) σ_t response of the AE42 samples under 40 fatigue cases: tension, torsion, and tension + torsion: $R^2 = 0.95$. Black line – the regression line.

Fig. 9. σ_t response of the AE42 samples.





(a) Profile of τ_t for the rubber part of the AE42 sample under tension 0 – 9.8 mm displacement and torsion angle 0 - 100° with failed number of 10000. (b) τ_t response of the AE42 samples 40 fatigue cases in tension, torsion, and tension + torsion: $R^2 = 0.95$. Black line – regression line.

Fig. 10. τ_t response of AE42 samples under the fatigue loadings.

2.2.4 τ_t application for AE42 samples

Figure 10(a) shows a profile of τ_t using the same load case for σ_t in section 2.2.3. The maximum value of τ_t is at the middle section. The response of τ_t for 40 fatigue cases is shown in Fig. 10 (b). The result has achieved a scatter band of 1.25 with $R^2 = 0.95$. The criterion τ_t obtained the same accuracy as that of σ_t .

2.3 Effect of geometrical shape on damage criteria

Both σ_t and τ_t were applied to AE2 and AE42 samples, respectively, and demonstrated the effectiveness in the prediction of fatigue damage in each type of specimen. There was a geometry difference between the two types of specimens. In this section, we try to explore the effect of the geometry on both σ_t and τ_t . Using the two regression lines calculated from AE2, that is, the lines in Fig. 7(d) and Fig. 8(e), together with the measured numbers of the failure cycles in AE42, we can obtain the predicted σ_t and τ_t of AE42. The other set of σ_t and τ_t in AE42 can be calculated from the finite element model of AE42 itself. Figures 11 (a) and (b) show comparisons of σ_t and τ_t , respectively. A scatter band of 1.5 with $R^2 = 0.94$ and a scatter band of 1.25 with $R^2 = 0.95$ were obtained, indicating a strong correlation between the responses of AE2 and AE42. Therefore, we can unify the responses of AE2 and AE42 to generate a single S-N curve for both samples. Figure 11 (c) shows the unified response of σ_t with a scatter band of 1.25 and $R^2 = 0.91$. The S-N curve can be expressed as:

$$\sigma_t = k N^{-m} \tag{19}$$

where

$$k = 56.8, m = 0.185 \tag{20}$$

Similarly, the S-N curve of τ_t can be written as:

$$\tau_t = k N^{-m} \tag{21}$$

where

$$k = 39.5, m = 0.186 \tag{22}$$

Figure 11(d) shows the S-N curve of τ_t with a scatter band of 1.25 and $R^2 = 0.90$. Further investigation indicates that there is a certain relationship between the fatigue strength σ_t and the shape change τ_t under cyclic loadings. Comparing function (19) with (21), we can relate τ_t to σ_t :

$$\tau_t = 0.7\sigma_t \tag{23}$$

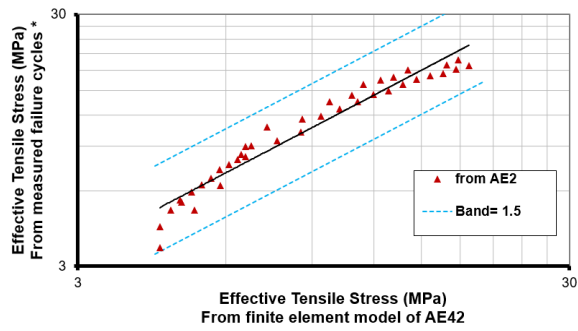
From the above investigation, the effectiveness of the proposed damage criteria appears not influenced by the change in geometry in different specimens; that is, the criteria can be applied to different components. In addition, the two criteria have produced closed results for fatigue life.

3. Discussion

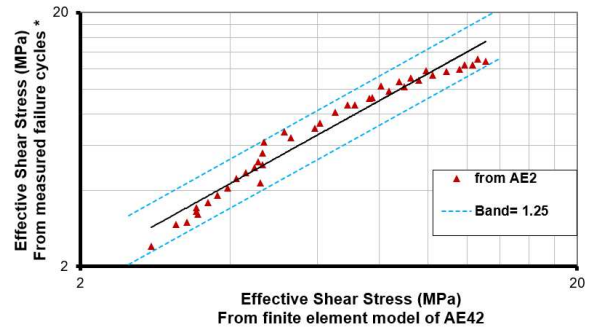
Ayoub et al. [23, 24] performed extensive fatigue tests with 168 cases in the AE2 and AE42 samples. They also developed an equivalent stress model to simulate fatigue damage. In this section, we benchmark three damage criteria, that is, the maximum tensile stress, the equivalent stress, and the effective tensile stress, to test their applicability for the prediction of rubber fatigue of AE2 samples under different R ratios.

First, a commonly used criterion, that is, maximum tensile stress, is tried. Figure 12 shows the comparison between the predicted and measured fatigue life. The maximum tensile stress criterion could not be used as an adequate fatigue parameter, since it could not unify the prediction in both tension and torsion experiments.

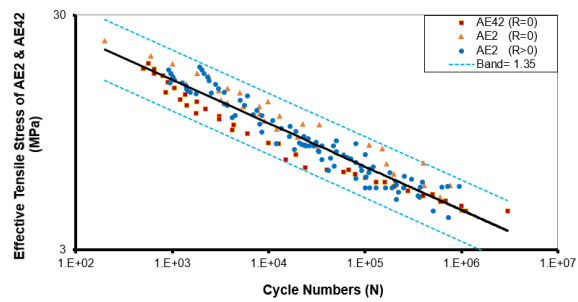




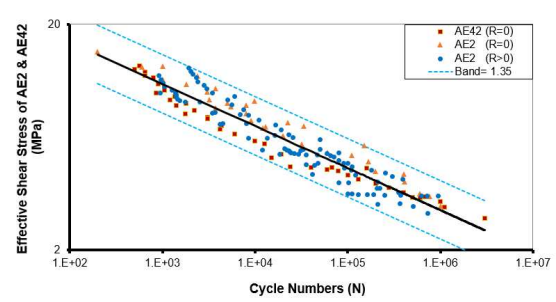
(a) Comparison between prediction from measured failed cycles and prediction from the AE42 finite element model: $R^2 = 0.94$. Black line – regression line.



(b) Comparison between prediction from failed cycles and prediction from AE42 finite element model: $R^2 = 0.95$. Black line – regression line.

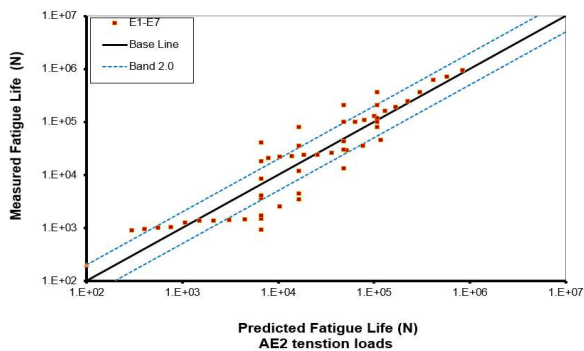


(c) σ_t response of 168 fatigue cases from both AE2 and AE42: $R^2 = 0.91$. Black line – regression line.

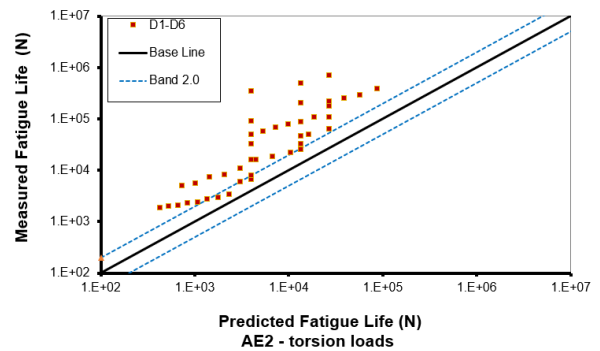


(d) τ_t response of 168 fatigue cases from AE2 and AE42: $R^2 = 0.90$. Black line – regression line.

Fig. 11. σ_t and τ_t response for AE2 and AE42 in all load cases.

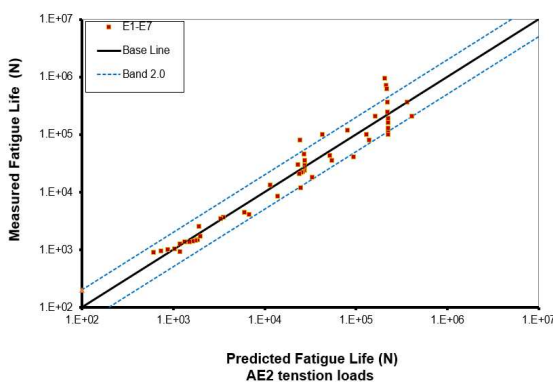


(a) Comparison of fatigue life between the prediction and the measurement using maximum tensile stress for AE2 under tension loads. Black line – regression line.

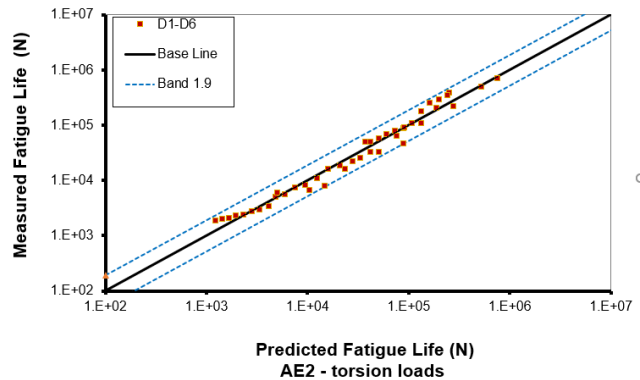


(b) Comparison of fatigue life between the prediction and the measurement using the maximum tensile stress for AE2 under torsion loads. Black line – regression line.

Fig. 12. Comparison of fatigue life using the maximum tensile stress criterion.



(a) Comparison of AE2 under tension loads. Black line – regression line.



(b) Comparison of AE2 under torsion loads. Black line – regression line.

Fig. 13. Comparison between the predicted and experimental fatigue life results of AE2 specimens using the effect tensile stress criterion.



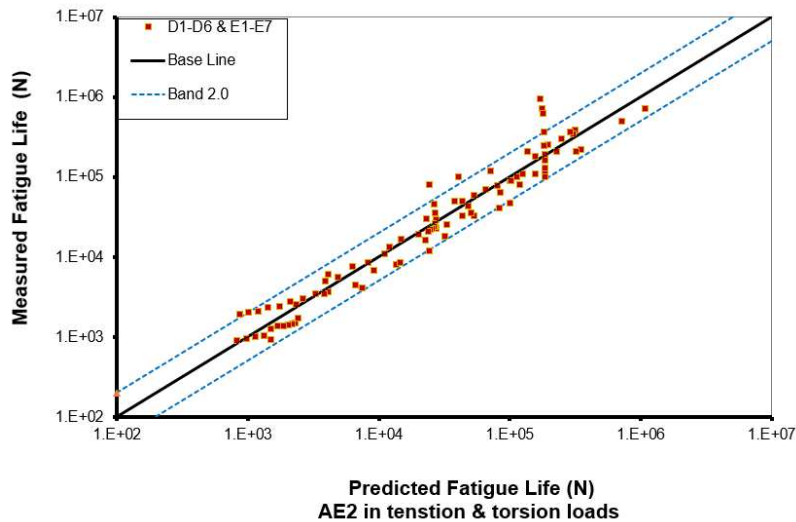


Fig. 14. Comparison between the predicted and experimental fatigue life results of AE2 samples using the effective stress criterion for both tension and torsion loads. Black line – regression line.

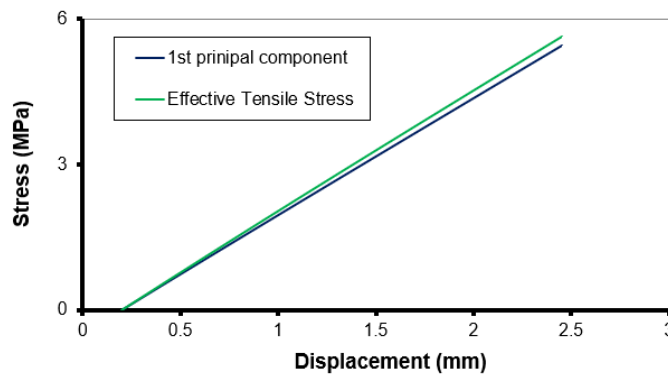


Fig. 15. Comparison between the effective tensile stress and its first principal component of the AE2 sample under a loading case: 0.2 mm to 2.45 mm in tension.

Second, the equivalent stress criterion was applied to AE2 samples in the tension loads and the torsion loads separately. The excellent results were obtained, and all the points were within a band factor of 3 [23]. However, since this criterion contains two adjustable parameters to be determined by specified fatigue data and is influenced by the sample geometry, its application to engineering design and application for different products requires extra work and more effort.

Third, the proposed effective tensile stress criterion is applied. The comparison between the prediction and the experiment is shown in Fig. 13. For tension loading, 83% of the points are within the band 2.0, which indicates good agreement. For torsional loading, all points are within the band 1.9, which shows excellent agreement. Hence, this criterion obtained a unified prediction for both loading modes and could be considered as a strong indicator.

Fourth, we plotted the comparison in both tension and torsion loads together, shown in Fig. 14. 90.5% of the points were located in the band of 2.0. This value demonstrates that the effective tensile stress criterion can unify both loading conditions. There was no equivalent plot of the equivalent stress found in the literature.

Finally, the assumption of the effective tensile stress criterion indicates that the compression stress would not generate fatigue damage, see equation (2). Therefore, the negative principal stress (stresses) was not included in the proposed damage criterion. This criterion has unified the experimental data well for both crystallising rubber [25] and non-crystallising rubber in this investigation. In addition, it is noted that the first principal component σ_{t1} contributes most of the fatigue damage, as shown in Fig. 15 for a typical loading case of the AE2 sample. Therefore, it would be possible to use σ_{t1} instead of σ_t here. This observation needs to be investigated further on more engineering applications to verify its applicability. We would report the progress in due course.

In summary, under the condition of different R ratios, the maximum stress criterion is not suitable. The equivalent stress criterion may be used to predict rubber fatigue provided that the two adjustable parameters can be determined accurately. The effective tensile stress criterion could be a strong indicator of fatigue prediction for non-crystallizing rubbers.

4. Conclusions

In this investigation, the recently developed criterion σ_t and the new damage criterion τ_t were first applied to non-crystallizing rubber using AE2 and AE42 specimens made from SBR under $R \geq 0$ conditions. Using 168 fatigue data, the criteria were validated and the relationship between shape and the fatigue strength was obtained. The main findings are summarised below.

- The proposed fatigue criteria are a potentially novel approach for noncrystallizing rubber.
- The maximum values of damage criteria σ_t and τ_t , determined from their three principal components under different load modes and R ratios in both AE2 and AE42, were located at crack locations observed in the experiments.



- The proposed criteria unified all the multiaxial experimental data in different loading modes and R ratios. Strong correlations between the prediction and the observed failure cycles with a range of $R^2 \geq 0.90$ in all predictions.
- Two S-N curves from 168 fatigue cases in a range of 2×10^2 - 3×10^6 cycles achieved the narrow scatter bands with a factor of 1.35.
- Both direct stresses and shear stresses can be considered for evaluating fatigue damage. These two criteria have shown the same effectiveness on the cases presented. The reader can have an option to use one of them in their fatigue design.

These criteria are relatively new, more cases, especially in industrial design and applications, are needed to compare their applicability in fatigue prediction. We will report on progress in due course.

Author Contributions

Not Applicable

Acknowledgments

Technical support from Jonathan Foster at Trelleborg Antivibration Solutions is greatly appreciated. The helpful comments from the reviewers are also appreciated.

Conflict of Interest

The author declares that they have no known competing financial interests or personal relationships that could have appeared to influence the work reported in this paper.

Funding

This research did not receive a specific grant from funding agencies in the public, commercial or non-profit sectors.

Data Availability Statement

Data supporting the findings of this study are available on a reasonable request, subjected to the company's approval.

References

- [1] Bourchak, M., Aid A., PE-HD fatigue damage accumulation under variable loading based on various damage models, *eXPRESS Polymer Letters*, 11, 2017, 117–126.
- [2] Liang, C., Gao, Z., Hong, S.K., Wang, G.L., Kwaku, Asafo-Duho B.M., Ren, J.Y., A Fatigue Evaluation Method for Radial Tire Based on Strain Energy Density Gradient, *Advances in Materials Science and Engineering*, 2021, 2021, 8534954.
- [3] Boulouar, A., Benseddiq, N., Merzoug, M., Benamara, N., Mazari M., A strain energy density theory for mixed mode crack propagation in rubber-like materials, *Journal of Theoretical and Applied Mechanics*, 54(4), 2016, 1417-1431.
- [4] Mars, W.V., Multiaxial fatigue crack initiation in rubber, *Tire Science and Technology*, 29, 2001, 171–185.
- [5] Mars, W.V., Kingston, J.G.R., Muhr, A., Martin, S., Wong, K.W., Fatigue life analysis of an exhaust mount. In: Austrell, P., and Kari, L., *Proceedings of the 4th European conference on the constitutive models for rubber*, 2005.
- [6] Mars, W.V., Fatemi, A., Nucleation and growth of small fatigue cracks in filled natural rubber under multiaxial loading, *Journal of Material Science*, 41, 2006, 7324–7332.
- [7] Xu, X., Zhou, X., Liu, Y., Fatigue life prediction of rubber-sleeved stud shear connectors under shear load based on finite element simulation, *Engineering Structures*, 227, 2021, 111449.
- [8] Belkhiria, S., Hamdi, A., Fathallah, R., Strain-based criterion for uniaxial fatigue life prediction for an SBR rubber: Comparative study and development, *Proceedings of the Institution of Mechanical Engineers, Part L: Journal of Materials: Design and Applications*, 234, 2020, 897–909.
- [9] Luo, R.K., Shear Criterion and Experimental Verification for Antivibration Fatigue Design, *Experimental Mechanics*, 62, 2022, 537–547.
- [10] Luo, R.K., Effective strain criterion under multimode and multiaxial loadings - a rubber S-N curve with the scatter-band factor of 1.6 from 90 fatigue cases, *eXPRESS Polymer Letters*, 16(2), 2022, 130-141.
- [11] Zerrin-ghalami, T., Fatemi, A., Fatigue life predictions of rubber components: Applications to an automobile cradle mount, *Proceedings of the Institution of Mechanical Engineers, Part D: Journal of Automobile Engineering*, 227, 2013, 691-703.
- [12] Shangquan, W.B., Duan, X., Liu, T., Wang, X., Zheng, G., Study on the Effect of Different Damage Parameters on the Predicting Fatigue Life of Rubber Isolators, *Journal of Mechanical Engineering*, 52, 2016, 116-126.
- [13] Luo, R., Wu, W.X., Cook, P.W., Mortel, W.J., An approach to evaluate the service life of rubber springs used in rail vehicle suspensions, *Journal of Rail and Rapid Transit*, 218, 2004, 173-177.
- [14] Verron, E., Prediction of fatigue crack initiation in rubber with the help of configurational mechanics. Austrell, P., Kari, L., *Proceedings of the 4th European conference on the constitutive models for rubber*, 2005.
- [15] Saintier, N., Cailletaud, G., Piques, R., Multiaxial fatigue life prediction for a natural rubber, *International Journal of Fatigue*, 28, 2006, 530–539.
- [16] Luo, R.K., Wu, W.X., Fatigue failure analysis of anti-vibration rubber spring, *Engineering Failure Analysis*, 13, 2006, 110-116.
- [17] Wu, W.X., Cook, P.W., Luo, R.K., Mortel, W.J., *Fatigue life investigation in the design process of metacone rubber springs*, *Elastomers and Components: Service Life Prediction – Progress and Challenges*, edited by Coveney, V., 2006.
- [18] Samad, M.S.A., Aidi, A., Sidhu, R.S., Durability of automotive jounce bumper, *Materials & Design*, 32, 2011, 1001-1005.
- [19] Luo, R.K., Effective Fatigue Evaluation on Rubber Mounts for Rail Vehicles, *Shock and Vibration*, 2021, 2021, 5574990.
- [20] Shangquan, W.B., Zheng, G.F., Liu, T.K., Duan, X.C., Rakheja, S., Prediction of fatigue life of rubber mounts using stress-based damage indexes, *Journal of Materials: Design and Applications*, 213, 2017, 657–673.
- [21] Mars, W.V., Fatemi, A., A Phenomenological Model for the Effect of R Ratio on Fatigue of Strain Crystallizing Rubbers, *Rubber Chemistry and Technology*, 76(5), 2003, 1241–1258.
- [22] Wang, X.L., Shangquan, W.B., Rakheja, S., Li, W.C., Yu, B., A method to develop a unified fatigue life prediction model for filled natural rubbers under uniaxial loads, *Fatigue & Fracture of Engineering Materials & Structures*, 37, 2014, 50-61.
- [23] Ayoub, G., Naït-Abdelaziz, M., Zaïri, F., Gloaguen, J.M., Charrier, P., Fatigue life prediction of rubber-like materials under multiaxial loading using a continuum damage mechanics approach: Effects of two-blocks loading and R ratio, *Mechanics of Materials*, 52, 2012, 87-102.
- [24] Ayoub, G., Naït-Abdelaziz, M., Zaïri, F., Multiaxial fatigue life predictors for rubbers: Application of recent developments to a carbon-filled SBR, *International Journal of Fatigue*, 66, 2014, 168-176.
- [25] Luo, R., Stress-Based S–N Base Function with Shear Modulus for Fatigue Assessment on Industrial Isolators, *Experimental Mechanics*, 62, 2022, 1059–1066.
- [26] Ogden, R.W., *Non-linear elastic deformations*, Chichester, UK, Ellis Horwood, 1984.
- [27] Abaqus user manual, Dassault Systems, 2020.
- [28] Luo, R.K., *Simulation methods for rubber antivibration systems*, World Scientific Publishing Co. Pte. Ltd, Singapore, 2020.



ORCID iD

Robert Keqi Luo  <https://orcid.org/0000-0002-2900-7316>



© 2023 Shahid Chamran University of Ahvaz, Ahvaz, Iran. This article is an open access article distributed under the terms and conditions of the Creative Commons Attribution-NonCommercial 4.0 International (CC BY-NC 4.0 license) (<http://creativecommons.org/licenses/by-nc/4.0/>).

How to cite this article: Luo R.K. Multimode Fatigue Criteria for Filled Non-crystalizing Rubber under Positive R Ratios, *J. Appl. Comput. Mech.*, 9(4), 2023, 1049–1059. <https://doi.org/10.22055/jacm.2023.43122.4027>

Publisher's Note Shahid Chamran University of Ahvaz remains neutral with regard to jurisdictional claims in published maps and institutional affiliations.

